



Article

Study on the Unsteady Flow Characteristics of a Pump Turbine in Pump Mode

Fei Zhang ¹, Zhenmu Chen ^{2,3,*}, Shuangqian Han ³ and Baoshan Zhu ^{3,*}

¹ Pumped-Storage Technological & Economic Research Institute, State Grid Xinyuan Company Ltd., Beijing 100761, China; spiritgiant@126.com

² Department of Mechanical and Electrical Engineering, Wenzhou University, Wenzhou 325000, China

³ Department of Energy and Power Engineering, Tsinghua University, Beijing 100084, China; hansq22@mails.tsinghua.edu.cn

* Correspondence: chenchenmu@163.com (Z.C.); bszhu@mail.tsinghua.edu.cn (B.Z.)

Abstract: Extensive research has been conducted on the performance of pump turbines, particularly focused on understanding the generation mechanism of S-shaped characteristics. However, there has been a lack of research on unsteady flow characteristics in hump characteristics with small guide vane openings. This study focuses on the hump characteristics of a pump turbine in pump mode. The unsteady numerical simulation method is used along with experimental testing to examine the internal flow characteristics and induced pressure fluctuations under pump operating conditions. The results indicate that flow separation occurs in the impeller when the flow rate decreases to the valley operating condition, and recirculation flow occurs near the impeller inlet at the partial flow rate. Moreover, the unstable flow on the positive slope exhibits a low-frequency characteristic of $0.15f_n$. The pressure fluctuation from the hub to shroud areas of the guide vane region diminishes sequentially. Notably, distinct vortex structures emerge at the draft tube cone section under the valley operating condition. These structures extend toward the elbow section of the draft tube as the flow rate decreases. This phenomenon generates low-frequency pressure fluctuation originating from the primary frequency of the vortex and dean vortex on the surface, located at $0.4 D$ of the draft tube under conditions of low flow rate.

Keywords: pump turbine; unsteady flow; pressure fluctuation; pump mode; hump characteristics



Citation: Zhang, F.; Chen, Z.; Han, S.; Zhu, B. Study on the Unsteady Flow Characteristics of a Pump Turbine in Pump Mode. *Processes* **2024**, *12*, 41. <https://doi.org/10.3390/pr12010041>

Academic Editor: Sergio Bobbo

Received: 23 November 2023

Revised: 16 December 2023

Accepted: 19 December 2023

Published: 22 December 2023



Copyright: © 2023 by the authors. Licensee MDPI, Basel, Switzerland. This article is an open access article distributed under the terms and conditions of the Creative Commons Attribution (CC BY) license (<https://creativecommons.org/licenses/by/4.0/>).

1. Introduction

Wind and solar energy production have experienced rapid global advancement [1]. However, due to their inherent variability, these energy sources pose challenges in providing a standalone power supply. In contrast, hydropower offers an effective means to mitigate fluctuations and minimize the impact of grid integration on stability thanks to its exceptional regulation capabilities and the ability of energy storage devices to store and release energy [2,3].

Pumped storage power plants, as a crucial component of hydropower, currently serve as a widely implemented energy storage technology and play an increasingly significant role in power systems [4,5]. During periods of low grid demand, pumped storage power plants operate as pumps, utilizing excess electricity from the grid to transfer water from the lower reservoir to the upper reservoir. Conversely, during periods of high grid demand, they function as turbines, using the water from the upper reservoir for power generation. In this way, pumped storage power plants fulfill the essential roles of regulating peak loads and filling valleys within the electricity grid.

The stable operation of the pump-turbine unit, as the core component of pumped storage power plants, directly affects the safety of the power plant [6,7]. The design of the pump-turbine unit must not only meet the requirements of pump operation but also consider the demands of turbine operation. This poses a challenge in ensuring optimal

performance in both pump and turbine conditions simultaneously. Due to the need to address these two operating conditions, pump-turbine units exhibit unstable characteristics, with the “S” characteristic and hump characteristic being particularly prominent.

The “S” characteristic arises during turbine operation, evident in the “S” shape displayed on the n_{11} – Q_{11} characteristic curve. The hump characteristic manifests during pump operation and is characterized by a positive slope on the flow–head curve [8–10]. However, it is challenging to avoid passing through the hump region during the pump operation startup process. In this range, one head corresponds to 2–3 flow rates, resulting in rapid fluctuations in flow rate. When the unit operates within this region, it experiences severe vibrations, intense noise, and a rapid surge in pressure fluctuations, ultimately affecting the unit’s normal operation [11].

Under off-design conditions, the efficiency of the pump deteriorates at a faster rate compared with the turbine. Moreover, there is a higher likelihood of flow separation in the deceleration and pressure increase flow during pump operation. As a result, the design of pump-turbine units typically focuses on meeting the requirements of pump operation, using turbine operation parameters as the basis for verification. With the increasing significance of pump-turbine units in load regulation and frequency regulation tasks, along with accelerated adjustment cycles, the unit is more susceptible to operating at low flow rates during pump conditions. This further compromises the safety and stability of the unit [12–16].

Li et al. [17,18] concluded that the hump characteristics near the optimum condition are mainly caused by an increase in hydraulic losses, while the hump characteristics away from the optimum condition are caused by a decrease in Eulerian energy and an increase in hydraulic losses. In other studies, the hysteresis characteristics of the hump area were found, and the hysteresis characteristics were investigated using Euler theory and hydraulic loss. The difference between Euler energy and hydraulic loss in the direction of flow increase and flow decrease leads to the hysteresis effect. The hysteresis phenomenon in the hump zone increases the range of the hump instability zone, which indicates that the design of the hump margin is insufficient [19]. Liu et al. [20] carried out a study on the cavitation characteristics and hump characteristics of a pump turbine. They found a certain relationship between the shape of the hump characteristics and the cavitation coefficient. The lower the cavitation coefficient, the less obvious the hump characteristics. Under the same guide vane opening, as the cavitation coefficient decreases, the hump characteristic will appear earlier. In other words, the generation of cavitation will inhibit the generation of the hump characteristic. Guo et al. [21] studied the effect of a leading-edge bulge on the hump characteristics of a pump turbine using three-dimensional steady-state simulation, and the numerical calculation results were in good agreement with the test. It was found that compared with the flow field of the original guide vane, the leading edge raised guide vane significantly improves the flow field in the guide vane area, which in turn improves the hump characteristics. Furthermore, the improvement in the flow field varies with the leading-edge bulges of different wave numbers and amplitudes.

Extensive research has been conducted on the performance of pump turbines, particularly focused on understanding the generation mechanism of S-shaped characteristics during the turbine mode. However, there has been a lack of research on unsteady flow characteristics in hump characteristics in the pump mode. The complexity of internal flow conditions, including guide vanes and stay vanes, leads to the occurrence of rotating stalls in the guide vane area during pump operation. Rotating stall generates low-frequency pressure fluctuation, a concept widely accepted in the field. Nevertheless, limited research has been conducted on the influence of other unstable flows on rotating stalls in pump turbines. Therefore, it is crucial to conduct a comprehensive study on the unstable flows within pump turbines. This article aims to analyze the causes of rotating stalls in the guide vane area using unsteady state analysis and provide a detailed understanding of its development process. Additionally, the effect of flow patterns in the impeller on the rotating stall is investigated.

2. Model and Method

2.1. Pump-Turbine Modeling

The head of the prototype of the pump turbine is 308 m, and the output power is 306.12 MW, which is designed for the Pushihe-pumped storage power station. The parameters of the model used for meshing are consistent with those of the test model. The main parameters of the pump-turbine model are shown in Table 1, and the impeller model of the test is shown in Figure 1. The pump-turbine model experiment was conducted on an IEC standard hydraulic machinery test rig within an uncertainty of 0.2% for efficiency. The S112A22 series pressure transducer was utilized to adapt the pressure signal. All the data were collected for 10 s after the pump-turbine operating condition was adjusted and stabilized.

Table 1. The parameters of pump turbine model.

Parameter	Value
Inlet diameter D_1 (m)	0.45
Outlet diameter D_2 (m)	0.27
Number of impeller blades Z	7
Number of stay vanes Z_s	20
Number of guide vanes Z_g	20
Design flow rate Q_{id} (m^3/s)	0.2439
Design head H_{id} (m)	28.2
Rated rotation speed n (r/min)	1000

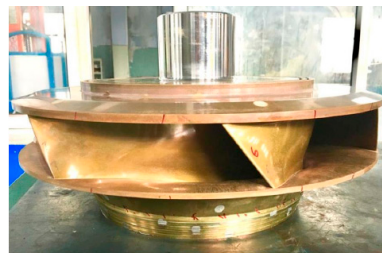


Figure 1. Pump turbine impeller for test.

The specific speed of the pump turbine is one of the important parameters to measure hydraulic performance. Usually, a pump operating under 1 m head flows $1 \text{ m}^3/\text{s}$ when the speed is called the specific speed n_q . Using a similar conversion, the relationship between the working parameters of the pump turbine can be obtained. Therefore, the specific speed of the pump turbine is defined as shown in Equation (1). The specific speed n_q of the pump turbine is 42, which belongs to the medium-specific speed pump turbine. Moreover, the Reynolds number of this pump turbine model is 3.8×10^4 , which is defined as shown in Equation (2).

$$n_q = \frac{n\sqrt{Q}}{H^{3/4}} \quad (1)$$

$$\text{Re} = \frac{D_2 u}{\nu} \quad (2)$$

2.2. Numerical Method

In this study, the ANSYS-CFX 18.0 [22] is used to calculate the internal flow characteristics of the pump turbine. The solutions of the N-S equations are shown in Equations (3) and (4) in this study.

$$\frac{\partial U_i}{\partial x_i} = 0 \quad (3)$$

$$\frac{\partial U_i}{\partial t} + U_j \frac{\partial U_i}{\partial x_j} = f_i - \frac{1}{\rho} \frac{\partial P}{\partial x_i} + \nu \frac{\partial^2 U_i}{\partial x_j^2} + \frac{1}{\rho} \frac{\partial (-\rho \overline{u_i' u_j'})}{\partial x_j} \quad (4)$$

Several operation conditions with different flow rates under a constant pump head are conducted. Therefore, the static pressure is used on the spiral casing outlet, and the mass flow rate is set on the draft tube inlet of the pump turbine with 5% of the turbulence intensity. The interface of the frozen rotor is used between the rotor and stator for the steady-state analysis and the interface of the transient rotor stator is used for the unsteady-state analysis. The walls are set in a no-slip condition. The shear stress transport (SST) turbulence model was developed by Menter [23–25]. The equations of SST are shown in Equations (5) and (6). This model provides better predictions of flow separation under reverse pressure gradients and is widely used in the calculation of pump turbines [26–30]. In this study, the SST turbulence model is selected for the CFD calculation. The steady flow calculation results are utilized as the initial condition for the unsteady state analysis to enhance convergence speed. Moreover, the root mean square values of the governing equation residuals were set to 0.0001 for all equations as the convergence criteria.

$$\frac{\partial}{\partial x_i} (\rho k u_i) = \frac{\partial}{\partial x_i} \left(\Gamma_k \frac{\partial k}{\partial x_j} \right) + \overline{G_k} - Y_k + S_k \quad (5)$$

$$\frac{\partial}{\partial x_i} (\rho \omega u_i) = \frac{\partial}{\partial x_i} \left(\Gamma_\omega \frac{\partial \omega}{\partial x_j} \right) + G_\omega - Y_\omega + D_\omega + S_\omega \quad (6)$$

The three-dimensional flow model of the pump turbine is used for the analysis. The computational domain is partitioned into several components, including the spiral casing, stay vane, guide vane, impeller, and draft tube, as shown in Figure 2. ANSYS-ICEM was utilized to generate the mesh of the spiral casing and draft tube. ANSYS-TurboGrid was used to generate the mesh of the guide vane, stay vane, and impeller. A mesh independence test was conducted, as shown in Figure 3. The result shows that the efficiency of the pump turbine approaches a constant after the mesh reaches a count of around 7 million. Therefore, the calculation with a grid count of 7.0×10^6 was utilized, as shown in Figure 4.

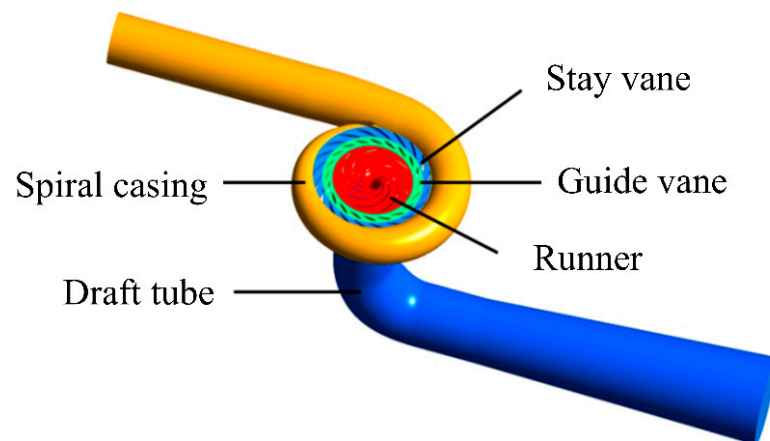


Figure 2. Three dimensions of the unsteady-state analysis.

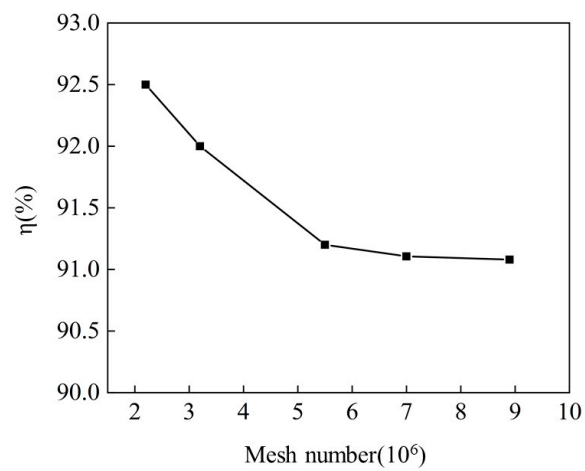


Figure 3. Grid independence validation.

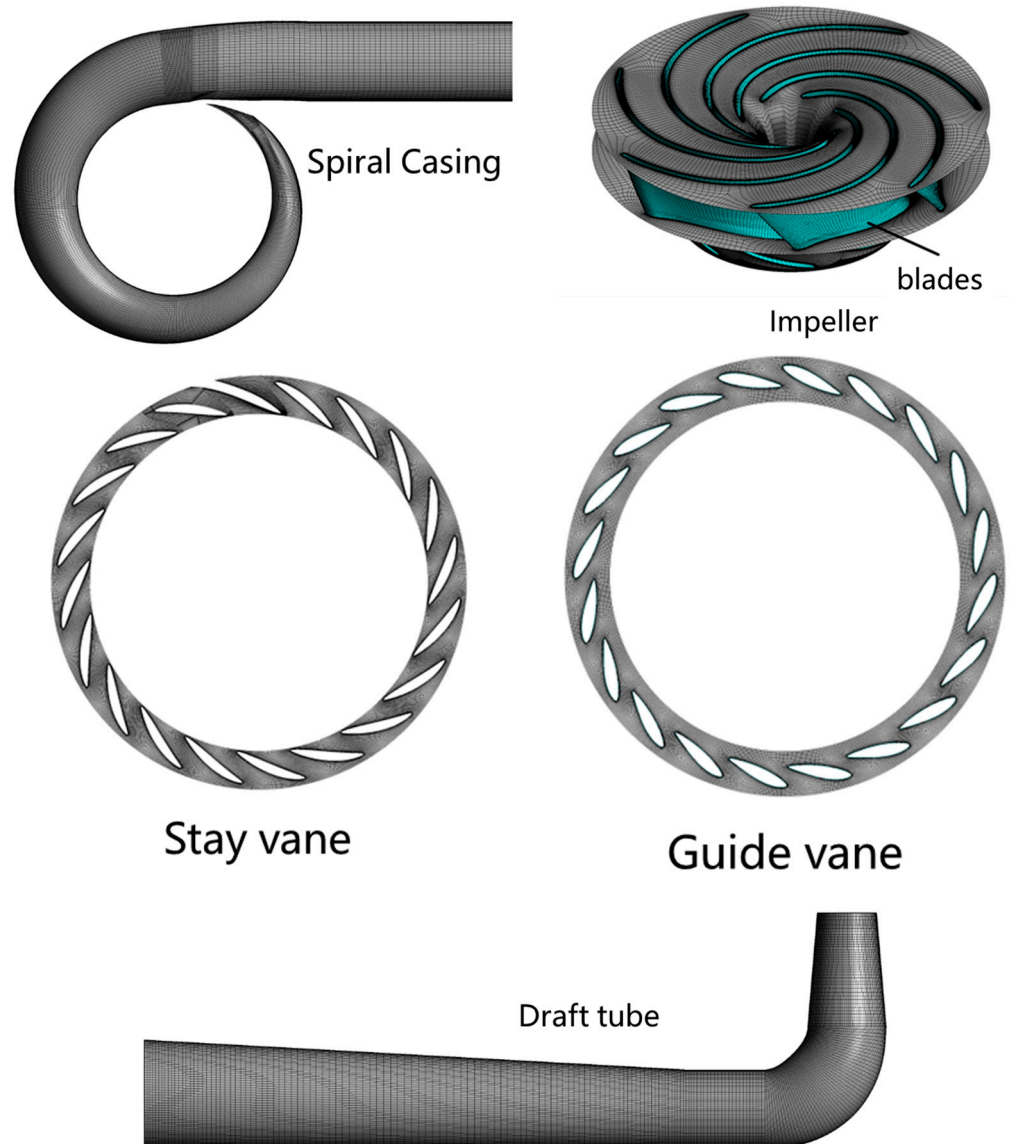


Figure 4. Final mesh for the unsteady-state analysis.

3. Results and Discussion

3.1. Performance of the Pump Turbine

The performance of the pump turbine in pump mode during the experiment is shown in Figure 5. The results show that the hump characteristic exists obviously under the condition with the flow rate of around 200 L/s with different guide vane openings. Moreover, in order to investigate the hump characteristics of the pump turbine under a small guide vane opening, a guide vane opening of 19 mm was selected for CFD analysis. The performance of the pump turbine in pump mode with CFD and the experimental results are shown in Figure 6. Eight different flow conditions of the pump turbine operating around the hump characteristics are selected to conduct the numerical analysis. The Q_0 is the flow rate of the pump turbine in pump mode with the best efficiency. The numerical simulation results of the pump head and efficiency are almost in good agreement with the experimental test results. The maximum error in both the head and the efficiency is under the condition of $0.89Q_0$, in which the relative error of the head is less than 5% and the relative error of the efficiency is less than 4%. The friction loss and leakage are ignored during the CFD calculation, and these factors could contribute to the difference between the simulations and experiments. Moreover, these errors fall within a reasonable range, which confirms the accuracy of the numerical simulation.

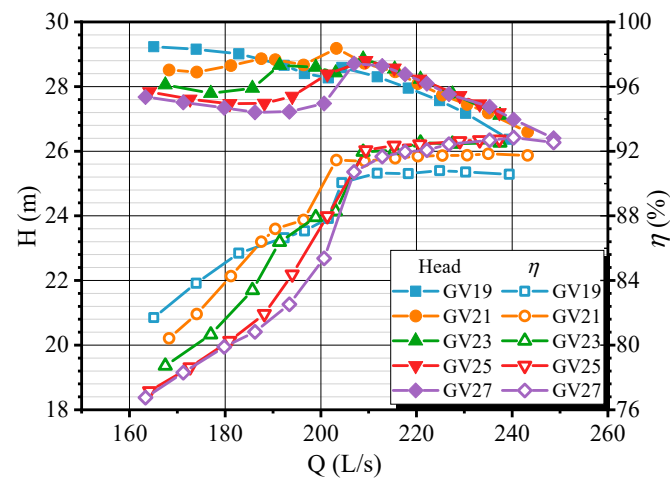


Figure 5. Performance of the pump turbine in pump mode during the experiment.

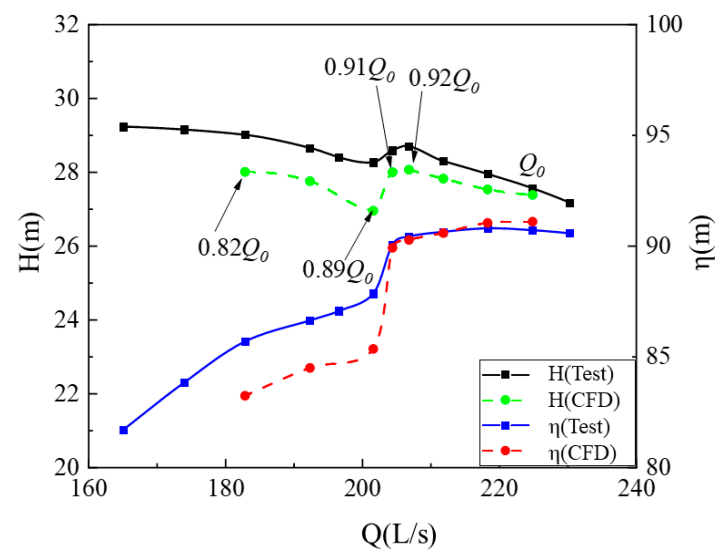


Figure 6. Comparison of test and simulation results.

3.2. Pressure Fluctuation Analysis

The pressure fluctuation in the vaneless space is generally the largest part of the pump turbine. The pressure fluctuation obtained from CFD and the experiment in the vaneless space is shown in Figure 7. According to the time-domain diagram, the characteristic frequency of the pressure fluctuation that is obtained with numerical calculation and the experiment is basically the same in the vaneless space. Because the compressibility of water is not considered in the CFD analysis, the amplitude of the pressure fluctuation in the CFD result is slightly smaller than that in the experimental result. From the frequency domain analysis, it can be observed that there are significant components of pressure fluctuation at $7f_n$, $14f_n$, $21f_n$, and $28f_n$. These components are caused by the periodic cutting of the impeller on the wakes of the guide vanes and the interaction between the rotor and stators. The amplitudes of these components increase with a decrease in the flow rate. Additionally, the pressure fluctuation with the components of $1f_n$ and $2f_n$ are also observed under the conditions of Q_0 and $0.91Q_0$, which is the impeller shaft frequency and its harmonic. These components are caused by unstable flow inside the impeller in the pump mode. Under the condition of $0.91Q_0$, a low-frequency component is also observed in both the numerical simulation and experimental analysis. The frequency of this low-frequency component is much lower than the frequencies of other components, and its amplitude is comparable to that of the $7f_n$ component. Moreover, the low-frequency component of $0.191f_n$ and $0.15f_n$ in the vaneless space under the flow rate of $0.91Q_0$ is found in the CFD and experimental results, respectively, which is induced by the rotating stall in the vaneless space. As the flow rate decreased to $0.89Q_0$, the intensity induced by the rotor-stator interaction continued to increase, and the amplitude of the low-frequency component of $0.15f_n$ induced by the rotating stall decreased. However, the amplitude of the $7f_n$ pressure fluctuation further increased under the flow rate of $0.82Q_0$. When the flow rate decreased to $0.82Q_0$, a significant low-frequency component is observed in the frequency domain, and the low-frequency of $0.131f_n$ in both the CFD and experimental analyses is obtained.

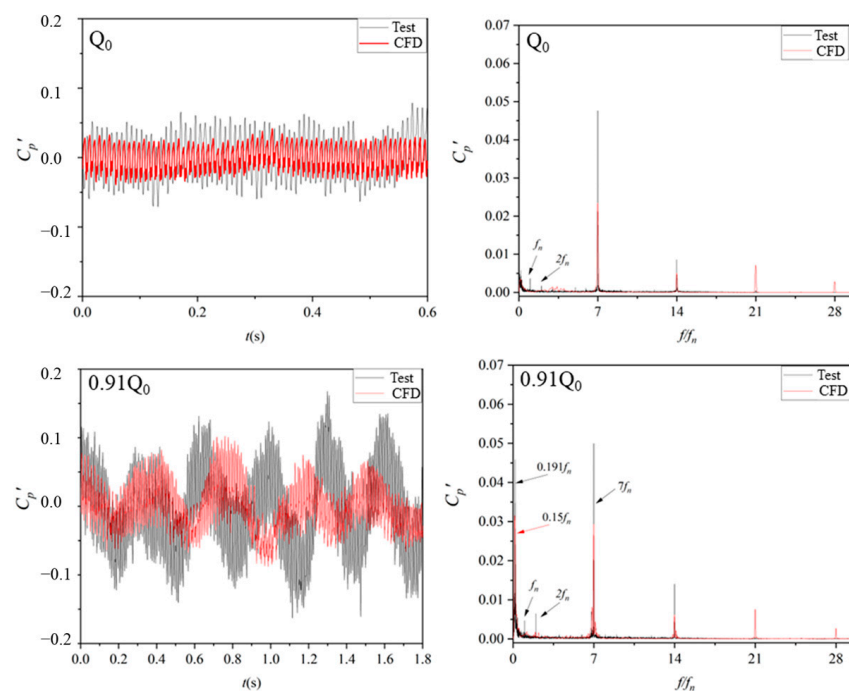


Figure 7. Cont.

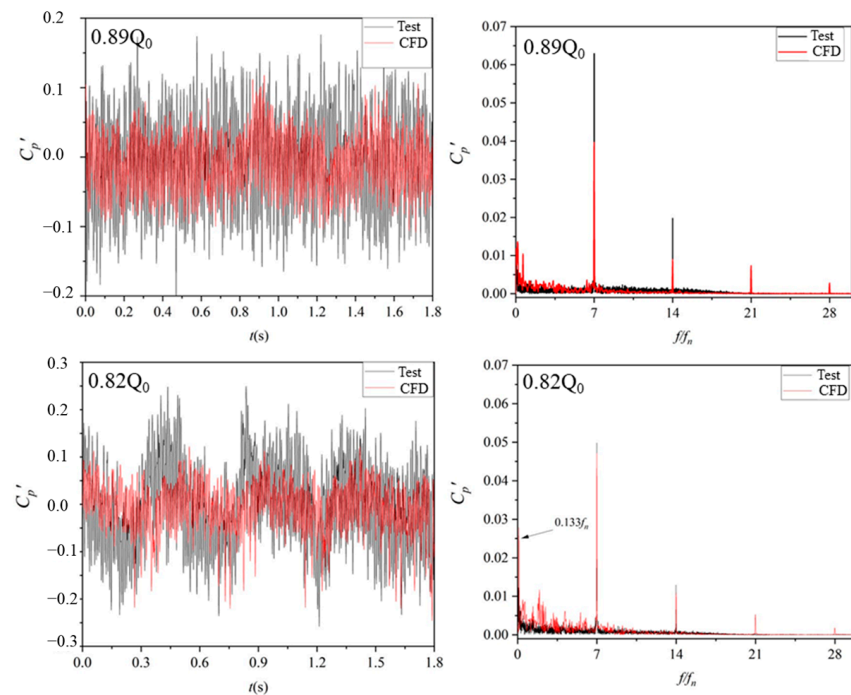


Figure 7. Pressure fluctuation analysis on the vaneless space.

To determine whether the frequencies of $0.15f_n$ and $0.133f_n$ in the $0.91Q_0$ and $0.82Q_0$ operating conditions are due to rotor stall, respectively, the pressure characteristics on the vaneless space were analyzed in detail. The pressure was extracted for analysis using bandpass filtering techniques, as shown in Figure 8. The red parallel lines approximate the propagation period of rotor stall, and the blue lines represent arbitrary times.

As the rotor rotates, the direction of rotor stall propagation is the same as the direction of rotation from GV01 to GV20. From Figure 8a, it can be seen that a single rotation stall propagated around the guide vane within 1.6 s. The blue lines intersect the four red parallel lines at any given time, indicating the presence of four rotational stall units in the guide vane, which means that the frequency of the rotating stall is $0.15f_n$. Figure 8b shows that a single rotation stall propagated around the circumferential direction of the guide vane within 1.8 s at $0.82Q_0$ operating conditions. The blue lines intersect the four parallel red lines at any given time, indicating the presence of four rotational stall units in the guide vane within a rotor cycle. Compared with Figure 8a, the propagation of the stall in the $0.82Q_0$ operating condition is less obvious than that in the $0.91Q_0$ condition. This is because, in the low flow rate condition, the flow in the guide vane area is more chaotic, which makes the propagation of the stall unstable.

To further determine the circumferential propagation speed and intensity of the rotor stall units in the $0.91Q_0$ and $0.82Q_0$ operating conditions, the pressure fluctuations at the four monitoring points GV01, GV06, GV11, and GV16 in the vaneless area were analyzed. It was found that GV01 was symmetrical with GV11 with respect to the rotation axis, and GV06 was symmetrical with GV16 with respect to the rotation axis. Figure 9a shows the bandpass pressure signals at the four measurement points at $0.15f_n$ in the $0.91Q_0$ operating condition. The phase difference between GV01 and GV11 is approximately 360 degrees, and the phase difference between GV06 and GV16 is also approximately 360 degrees, while the phase difference between GV06 and GV11 is approximately 360 degrees. This indicates that there are four rotational stall units in the non-bladed area under this operating condition, which is same with the fluctuation analysis results in Figure 8. The amplitude of the $0.15f_n$ frequency is different in the four directions, indicating that the intensity of a rotational stall is not the same at different circumferential positions.

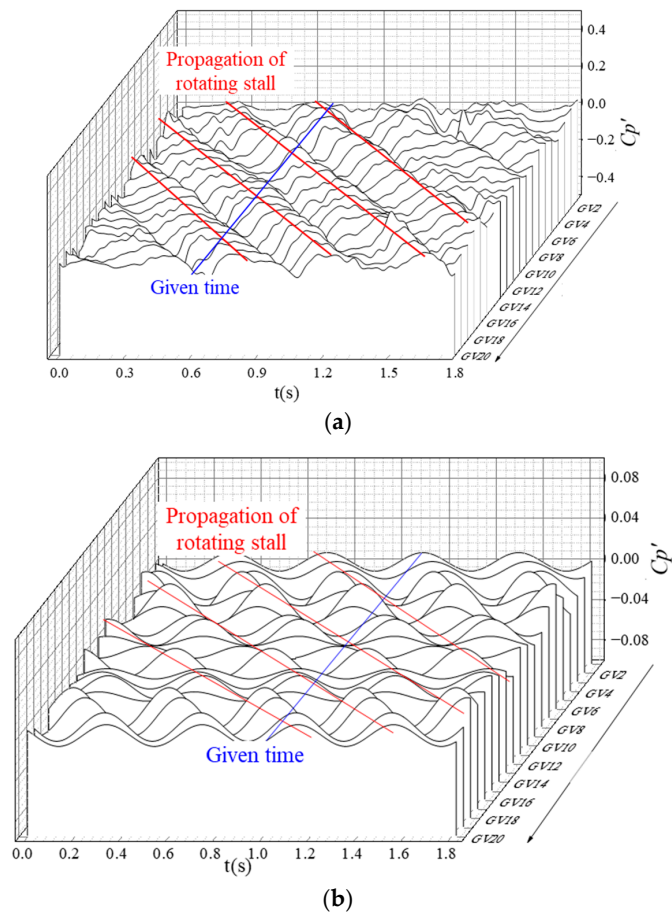


Figure 8. Time domain of the pressure fluctuation in the vaneless space. (a) $0.91Q_0$, (b) $0.82Q_0$.

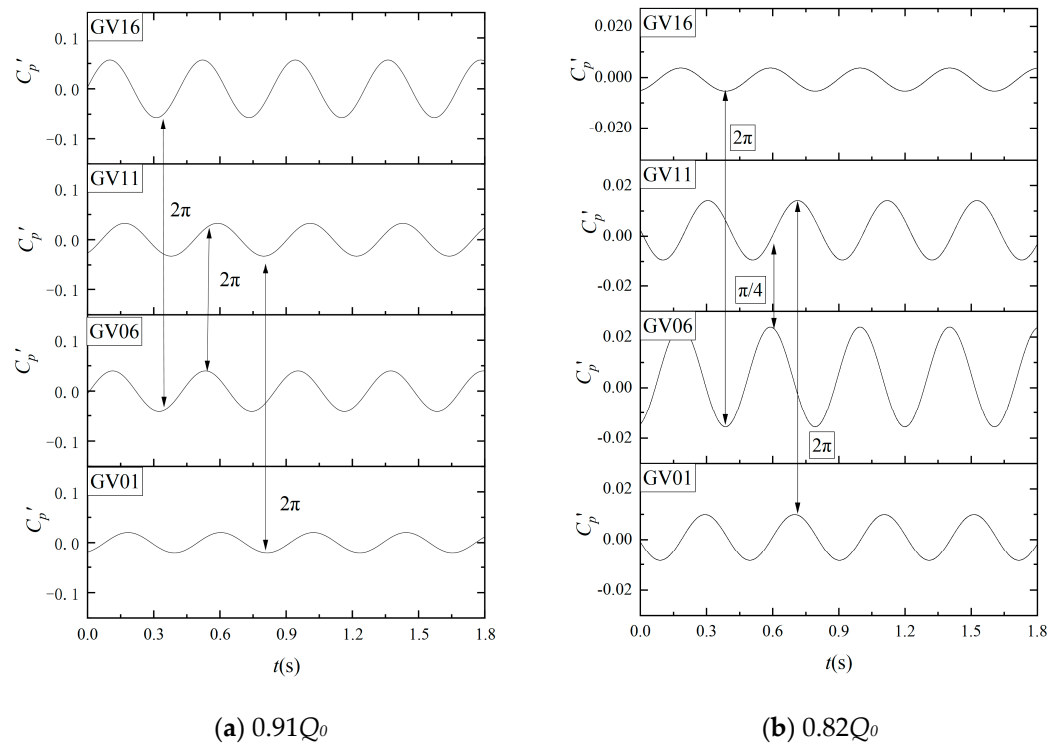


Figure 9. Filtered pressure fluctuation in the guide passage.

Figure 9b shows the bandpass pressure signals at the four measurement points at $0.133f_n$ in the $0.82Q_0$ operating condition. The phase difference between GV01 and GV11 is approximately 360 degrees, while the phase difference between GV06 and GV16 is also approximately 360 degrees, and the phase difference between GV06 and GV11 is about 45 degrees, indicating that the rotational stall units in the guide vane area are not evenly distributed in the circumferential direction at $0.82Q_0$. The amplitude of $0.131f_n$ is highest at GV06 and lowest at GV16, indicating that the intensity of the rotational stall is stronger at GV06 and weaker at GV16.

With the analysis of pressure fluctuations, it was shown that the low-frequency components in the vaneless area under both the $0.91Q_0$ and $0.82Q_0$ operating conditions are caused by a rotational stall in the guide vane area. The frequency of the low-frequency component is different due to the different circumferential propagation velocities of the rotational stall in the two operating conditions.

Four monitoring points were evenly set up in the cone wall of the draft tube, as shown in Figure 10. The pressure fluctuation in the pump-turbine draft tube is shown in Figure 11. It can be observed that under the same operating conditions, the pressure fluctuations at the four monitoring points of the draft tube exhibit certain similarities. Each operating condition has components such as $7f_n$, $14f_n$, and $21f_n$, which are frequencies generated by the interaction between the impeller blades and the guide vanes. Due to the relatively stable internal flow under the condition of Q_0 , the components in the frequency domain mainly consist of the interaction frequencies between the rotator and stationary parts as well as their harmonics. A significant low-frequency component of $0.15f_n$ appears in the draft tube with the condition of $0.91Q_0$, which is induced in the vaneless space by a rotating stall. Therefore, this low-frequency component propagates downstream from the vaneless space to the draft tube. But the amplitude of the low-frequency component is reduced and is only approximately 30% of that in the vaneless space. Due to the formation of complex vortex structures at the draft tube, the frequency domain spectra of the $0.89Q_0$ and $0.82Q_0$ conditions have rich signals, and the amplitude of pressure fluctuations increases rapidly. Moreover, the diminishing impact of pressure fluctuations are caused by the interaction between the rotator and stator in the vaneless space on the draft tube.

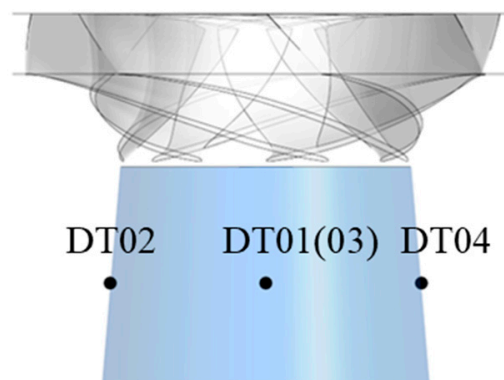


Figure 10. Locations for pressure monitor.

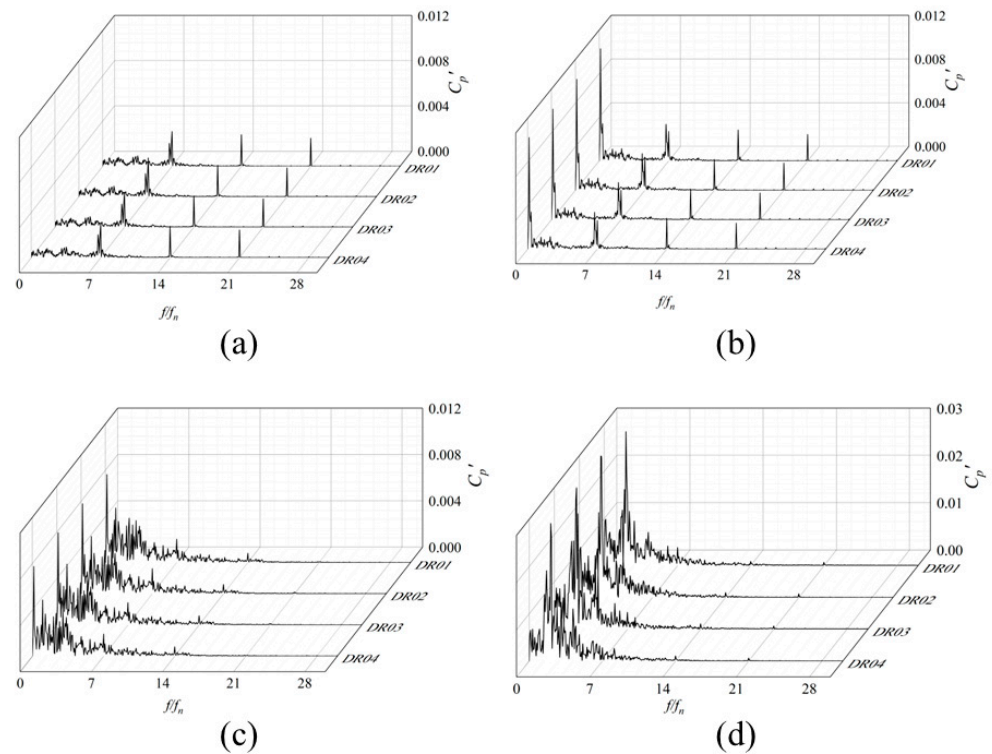


Figure 11. Pressure fluctuations in the draft tube. (a) Q_0 , (b) $0.91Q_0$, (c) $0.89Q_0$, and (d) $0.82Q_0$.

3.3. Internal Flow Characteristics

The streamline distribution of different spans within the impeller flow passage is shown in Figure 12. The flow distribution of the three spans is relatively uniform, and there is no apparent flow separation under the conditions of Q_0 and $0.91Q_0$, which means that there is no unsteady flow in the impeller passage when the flow rate is close to the best efficiency point condition. However, there is an obvious flow separation phenomenon at the span 0.1 of the impeller inlet under the condition of $0.89Q_0$. The vortex generated blocks the flow near the impeller shroud. Moreover, the flow separation phenomenon at the span 0.1 of the impeller is further enhanced under the condition of $0.82Q_0$, and the range of unstable flow extends to the impeller inlet.

When the pump turbine operates in pump mode, the draft tube serves as the inlet for the water flow, and the internal flow pattern in the draft tube can affect the downstream flow. Figure 13 shows the streamline distribution in the draft tube straight cone section under four different operating conditions. It can be observed that the streamlined distribution is uniform under the conditions of Q_0 and $0.91Q_0$, indicating a relatively stable flow pattern when the pump turbine operates close to the best efficiency condition. However, when the flow rate decreases to $0.89Q_0$, there is a slight distortion of the streamlines near the draft tube outlet. Under the flow rate of $0.82Q_0$, significant separation flow occurs at the impeller inlet, and the water flow recirculates along the draft tube from the impeller shroud side. Figure 14 illustrates the vortex structure in the draft tube. It can be seen that the recirculation at the impeller inlet forms complex vortex structures. Moreover, the vortex structures extend toward the draft tube as the flow rate decreases. The vortex structure extends to the longest from the impeller inlet under the condition of $0.82Q_0$.

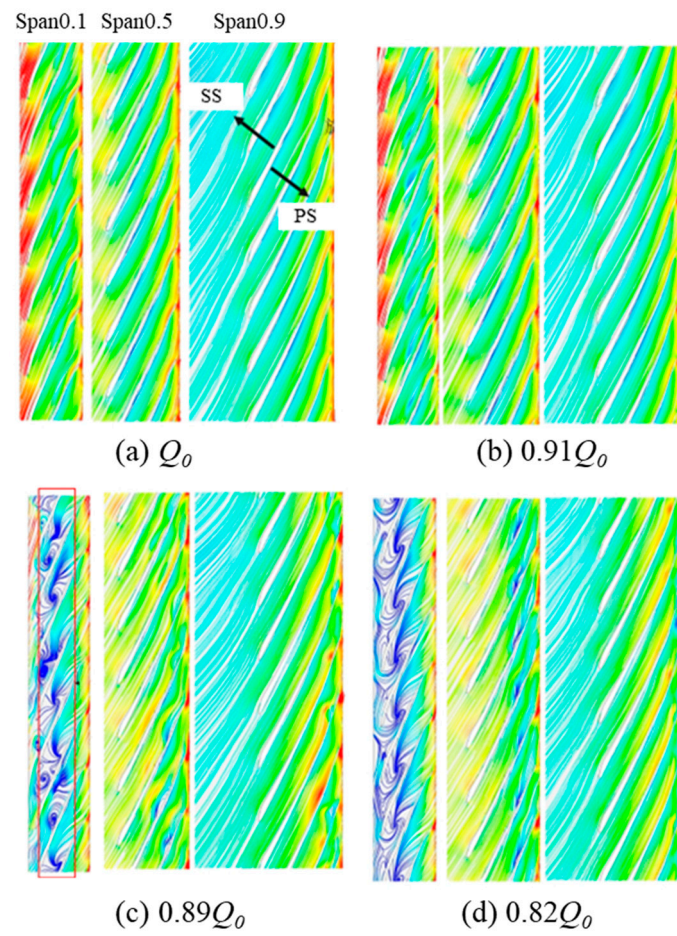


Figure 12. Streamline and pressure in different spans.

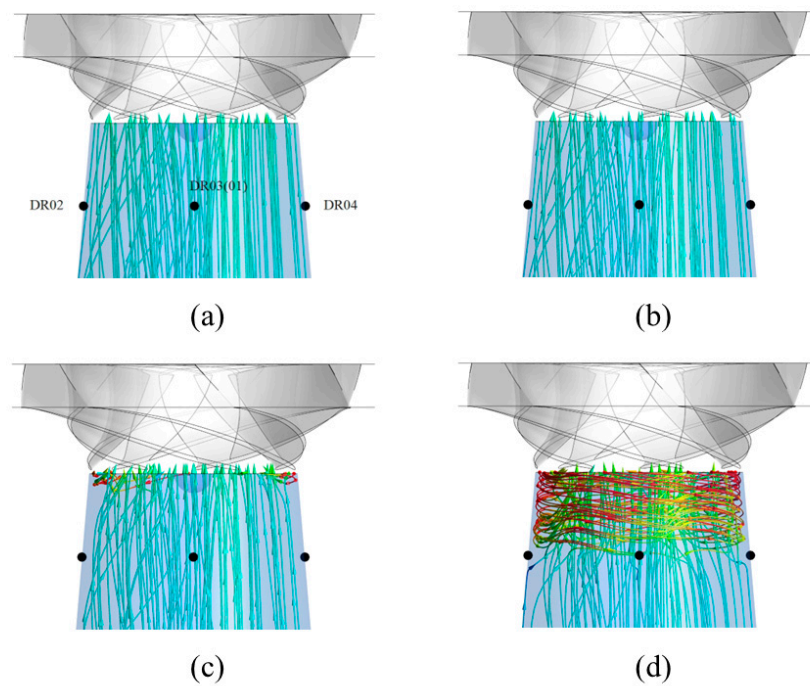


Figure 13. Streamline distribution in the draft tube. (a) Q_0 , (b) $0.91Q_0$, (c) $0.89Q_0$, and (d) $0.82Q_0$.

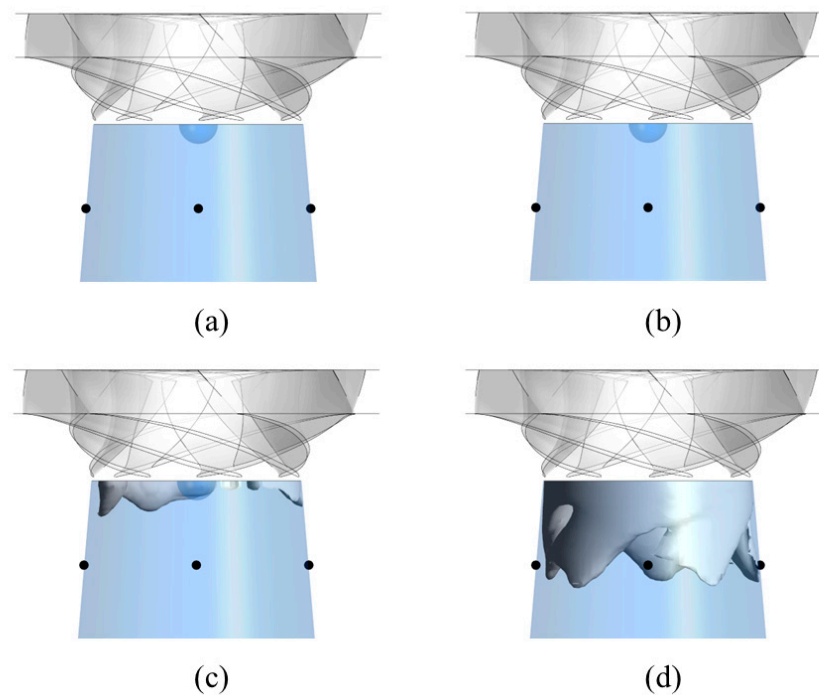


Figure 14. Vorticity distribution in the draft tube. (a) Q_0 , (b) $0.91Q_0$, (c) $0.89Q_0$, and (d) $0.82Q_0$.

4. Conclusions

In this study, the internal flow characteristics of a pump turbine in the hump region under the pump mode are investigated. The unsteady numerical simulation method is combined with experimental results. The pressure fluctuation and internal flow characteristics under the optimal condition (Q_0), positive slope condition ($0.91Q_0$), valley condition ($0.89Q_0$), and low flow condition ($0.82Q_0$) are discussed in detail.

- (1) Under the optimal condition with a flow rate of Q_0 , the flow instability in the vaneless space is mainly caused by the interaction between the rotor and stator, in which the pressure fluctuation is $7f_n$. The intensity of the pressure fluctuation of $7f_n$ increases when the flow rate decreases from Q_0 to $0.89Q_0$, and it achieves the largest extent under the flow rate of $0.89Q_0$. However, the intensity of the pressure fluctuation of $7f_n$ decreases when the flow rate further decreases to $0.82Q_0$.
- (2) A low-frequency component is found in the vaneless space of the pump turbine with the flow rate conditions from $0.91Q_0$ to $0.82Q_0$, which is caused by a rotating stall. A rotating stall in the vaneless space results in an uneven circumferential pressure distribution, and the number of rotating stalls is four for both flow rate conditions of $0.89Q_0$ and $0.91Q_0$. The intensity of each rotating stall remains the same and uniformly distributed in the vaneless space at the flow rate of $0.91Q_0$. However, the flow in the vaneless space is more chaotic in the low-flow rate condition of $0.82Q_0$, which makes the propagation of the stall unstable.
- (3) The flow pattern in the draft pipe is gradually chaotic with the decrease in flow rate in the pump mode. The main frequency of pressure fluctuation in the draft pipe is $7f_n$, propagating from the vaneless space under the condition of Q_0 . When the flow reaches the valley condition ($0.89Q_0$), the flow direction at the draft tube close to the impeller inlet is distorted. At lower flow rate conditions, backflow occurs in the draft tube, and the vortex develops along the wall of the draft tube toward the elbow part.

Author Contributions: Formal analysis, F.Z. and S.H.; Investigation, Z.C.; Data curation, S.H.; Writing—original draft, F.Z.; Writing—review & editing, Z.C. and B.Z.; Visualization, B.Z.; Funding acquisition, B.Z. All authors have read and agreed to the published version of the manuscript.

Funding: This research was supported by the Science and Technology Project of State Grid Xinyuan Group Company Limited (SGXYKJ-2023-053).

Data Availability Statement: Data are contained within the article.

Conflicts of Interest: Author Fei Zhang was employed by the company State Grid Xinyuan Company Ltd. The remaining authors declare that the research was conducted in the absence of any commercial or financial relationships that could be construed as a potential conflict of interest.

Nomenclature

CFD	computational fluid dynamics
D_1	inlet diameter
D_2	outlet diameter
f_n	rotational frequency
H	head
n	rotational speed
n_q	specific speed
Q	flow rate
Q_0	flow rate with best efficiency
Re	Reynolds number
t	time
u	velocity
Z	impeller blade number
Z_g	guide vane number
Z_s	stay vane number
η	efficiency
ν	kinematic viscosity

References

- Xu, L.; Liu, D.; Liu, X.; Wang, X. Review of pressure pulsation in bladeless area of high head pump turbine. *Hy-Dropower Pumped Storage* **2020**, *6*, 248–256.
- Kook, K.S.; McKenzie, K.; Liu, Y.; Atcitty, S. A study on applications of energy storage for the wind power operation in power systems. In Proceedings of the 2006 IEEE Power Engineering Society General Meeting, Montreal, QC, Canada, 18–22 June 2006.
- Blakers, A.; Stocks, M.; Lu, B.; Cheng, C. A review of pumped hydro energy storage. *Prog. Energy* **2021**, *3*, 022003. [[CrossRef](#)]
- State Grid Xinyuan Holdings Co. LTD. Pumped storage unit and auxiliary equipment technology. In *Pump Turbine*; China Electric Power Press: Beijing, China, 2019.
- Chen, S. *Numerical Study on Water Ring Characteristics of Pump Turbine under Pressure Water Phase Regulation*; Xihua University: Chengdu, China, 2021.
- Zheng, X. *Research on Vibration Mechanism of Prototype Reversible Pump-Turbine*; North China Electric Power University: Beijing, China, 2018.
- Zhao, C. *Research on Stability of Pump Turbine under Runaway Condition*; Lanzhou University of Technology: Lanzhou, China, 2019.
- Li, D.; Song, Y.; Lin, S.; Wang, H.; Qin, Y.; Wei, X. Effect mechanism of cavitation on the hump characteristic of a pump-turbine. *Renew. Energy* **2021**, *167*, 369–383. [[CrossRef](#)]
- Yang, G.; Shen, X.; Shi, L.; Zhang, D.; Zhao, X.; van Esch, B. Numerical investigation of hump characteristic improvement in a large vertical centrifugal pump with special emphasis on energy loss mechanism. *Energy* **2023**, *273*, 127163. [[CrossRef](#)]
- Jia, J.; Zhang, J.; Qu, Y.; Cai, H.; Chen, S. Study on hump characteristics of pump turbine with different guide vane exit angles. *IOP Conf. Ser. Earth Environ. Sci.* **2019**, *240*, 072038. [[CrossRef](#)]
- Sun, Y. *Research on Hump Stability and Its Influencing Factors of Low Specific Speed Pump-Turbine*; Tsinghua University: Beijing, China, 2016.
- Shang, L.; Cao, J.; Wang, Z.; Liu, X. Hydraulic Characterization of Variable-Speed Pump Turbine under Typical Pumping Modes. *Processes* **2023**, *11*, 2903. [[CrossRef](#)]
- Hu, W.; Wang, Z.; Fan, H. Grid synchronization of variable speed pump-turbine units in turbine mode. *Renew. Energy* **2021**, *173*, 625–638. [[CrossRef](#)]
- Liu, Y.; Tan, L. Tip clearance on pressure fluctuation intensity and vortex characteristic of a mixed flow pump as turbine at pump mode. *Renew. Energy* **2018**, *129*, 606–615. [[CrossRef](#)]
- Lei, T.; Zhiyi, Y.; Yun, X.; Yabin, L.; Shuliang, C. Role of blade rotational angle on energy performance and pressure fluctuation of a mixed-flow pump. *Proc. Inst. Mech. Eng. Part A J. Power Energy* **2017**, *231*, 227–238. [[CrossRef](#)]

16. Zhao, X.; Xiao, Y.; Wang, Z.; Lou, H.; Soo-Hwang, A.; Yao, Y.; Fan, H. Numerical analysis of non-axisymmetric flow characteristic for a pump-turbine impeller at pump off-design condition. *Renew. Energy* **2018**, *115*, 1075–1085. [[CrossRef](#)]
17. Li, D.; Gong, R.; Wang, H.; Xiang, G.; Wei, X.; Qin, D. Entropy production analysis for hump characteristics of a pump turbine model. *Chin. J. Mech. Eng.* **2016**, *29*, 803–812. [[CrossRef](#)]
18. Li, D.; Wang, H.; Chen, J.; Nielsen, T.K.; Qin, D.; Wei, X. Hysteresis Characteristic in the Hump Region of a Pump-Turbine Model. *Energies* **2016**, *9*, 620. [[CrossRef](#)]
19. Li, D.; Wang, H.; Qin, Y.; Wei, X.; Qin, D. Numerical simulation of e characteristic in the hump region of a pump-turbine model. *Renew. Energy* **2018**, *115*, 433–447. [[CrossRef](#)]
20. Liu, D.-M.; Xu, W.-L.; Zhao, Y.-Z. Experimental study of the flow field of a high head model pump turbine based on PIV technique. *J. Hydrodyn.* **2021**, *33*, 1045–1055. [[CrossRef](#)]
21. Guo, Z.; Wang, C.; Qian, Z.; Luo, X.; Xia, W. Suppression of hump characteristic for a pump-turbine using leading-edge protuberance. *Proc. Inst. Mech. Eng. Part A J. Power Energy* **2019**, *234*, 187–194. [[CrossRef](#)]
22. ANSYS Inc. ANSYS CFX Documentation, Ver. 18. Available online: <https://www.ansys.com> (accessed on 1 September 2020).
23. Menter, F.R. *Improved Two-Equation k- ω Turbulence Models for Aerodynamic Flows*; NASA Technical Memorandum TM 103975; NASA Ames: Moffett Field, CA, USA, 1992.
24. Menter, F.R. Two-equation eddy-viscosity turbulence models for engineering applications. *AIAA J.* **1994**, *32*, 1598–1605. [[CrossRef](#)]
25. Menter, F.R. Eddy Viscosity Transport Equations and Their Relation to the k- ϵ Model. *J. Fluids Eng.* **1997**, *119*, 876–884. [[CrossRef](#)]
26. Chen, Z.; Jiang, Z.; Chen, S.; Zhang, W.; Zhu, B. Experimental and numerical study on flow instability of pump-turbine under runaway conditions. *Renew. Energy* **2023**, *210*, 335–345. [[CrossRef](#)]
27. Pang, S.; Zhu, B.; Shen, Y.; Chen, Z. Study on cavitating vortex rope characteristics of reversible pump-turbine under part load turbine condition. *Phys. Fluids* **2023**, *35*, 085131. [[CrossRef](#)]
28. Li, D.; Wang, H.; Xiang, G.; Gong, R.; Wei, X.; Liu, Z. Unsteady simulation and analysis for hump characteristics of a pump turbine model. *Renew. Energy* **2015**, *77*, 32–42. [[CrossRef](#)]
29. Pang, S.; Zhu, B.; Shen, Y.; Chen, Z. S-shaped characteristics of pump turbine with large guide vane opening by experimental and numerical analysis. *AIP Adv.* **2023**, *13*, 015201. [[CrossRef](#)]
30. Li, Z.; Wang, Z.; Wei, X.; Qin, D. Flow Similarity in the Rotor–Stator Interaction Affected Region in Prototype and Model Francis Pump-Turbines in Generating Mode. *J. Fluids Eng.* **2016**, *138*, 061201. [[CrossRef](#)]

Disclaimer/Publisher’s Note: The statements, opinions and data contained in all publications are solely those of the individual author(s) and contributor(s) and not of MDPI and/or the editor(s). MDPI and/or the editor(s) disclaim responsibility for any injury to people or property resulting from any ideas, methods, instructions or products referred to in the content.